Molecular Catalysis 442 (2017) 191–201

Contents lists available at ScienceDirect

Molecular Catalysis

journal homepage: www.elsevier.com/locate/mcat

MCAT

Editor's choice paper

# Mesoporous $Pd_xPt$ alloys: High-performance catalysts for methane combustion

Xingtian Zhao, Yuxi Liu*, Jiguang Deng*, Peng Xu, Jun Yang, Kunfeng Zhang, Zhuo Han, Hongxing Dai*

*Beijing Key Laboratory for Green Catalysis and Separation, Key Laboratory of Beijing on Regional Air Pollution Control, Laboratory of Catalysis Chemistry and Nanoscience, Department of Chemistry and Chemical Engineering, College of Environmental and Energy Engineering, Beijing University of Technology, Beijing 100124, China*

ARTICLE INFO

*Article history:*
Received 23 June 2017
Received in revised form 18 August 2017
Accepted 2 September 2017

*Keywords:*
Mesoporous Pd–Pt alloy
PdO–$PtO_2$ active site
Redox property
Methane combustion
Methane activation ability

ABSTRACT

Mesoporous cubic $Pd_xPt$ ($x$ = 0.43–8.52) alloys with surface areas of 26–32 $m^2/g$ were synthesized using the KIT-6-templating method. Physicochemical properties of the materials were characterized by means of various techniques, and their catalytic activities were evaluated for methane combustion. It is found that the Pd and Pt were uniformly distributed in the $Pd_xPt$ alloys. The addition of Pt to Pd exerted a significant effect on the redox property of Pd. The $Pd_xPt$ alloys possessed a higher methane activation ability than the monometallic Pd. The oxidized Pd–Pt (i.e., PdO–$PtO_2$) were more active than the metallic $Pd^0$–$Pt^0$. The $Pd_{2.41}Pt$ sample performed the best for methane combustion ($T_{10\%}$, $T_{50\%}$, and $T_{90\%}$ were 272, 303, and 322 °C at SV = 100,000 mL/(g h); $TOF_{Pd}$, $TOF_{Pt}$, $TOF_{Pd+Pt}$, and specific reaction rate at 280 °C were $0.85 \times 10^{-3}$ $s^{-1}$, $1.98 \times 10^{-3}$ $s^{-1}$, $0.59 \times 10^{-3}$ $s^{-1}$, and 4.46 μmol/($g_{cat}$ s), respectively). The deactivation of the $Pd_{2.41}Pt$ sample induced by 2.5–5.0 vol% $CO_2$ or $H_2O$ addition was reversible, but its deactivation due to 100 ppm $SO_2$ introduction was irreversible. It is concluded that the excellent catalytic performance of the $Pd_{2.41}Pt$ sample was associated with its good mesoporous structure, Pd–Pt alloy and PdO–$PtO_2$ coexistence, and good methane and oxygen activation ability.



## 1. Introduction

Methane is widely used in industrial and transportation activities as it is the main component of natural gas. Due to its tough combustion, however, unburned methane at low temperatures always exists in the exhaust. It is generally accepted that methane induces a strong greenhouse effect with a global warming potential 20 times higher than that of $CO_2$ [1]. Therefore, much attention has been paid on reducing the emission of methane. Flame combustion of methane at high temperatures often results in the emissions of nitrogen oxides ($NO_x$) and CO that are harmful to the environment. Compared to the conventional flame combustion, catalytic combustion of methane is regarded as an efficient and green pathway, in which the key issue is the availability of high-performance catalysts at low temperatures. Therefore, it is highly desirable to design and prepare novel catalysts with excellent low-temperature activity and stability.

In the past years, the Pd-based catalysts have been investigated intensively and extensively due to their good catalytic performance for methane combustion [2–5]. For example, PdO or Pd–PdO mixture were recognized as the active phase of the supported Pd catalysts at low temperatures, but the metallic $Pd^0$ was the active phase at high temperatures [1–3,6,7]. The performance of the Pd-based catalysts for methane lean-burn combustion at low temperatures could be improved if the Pd was alloyed with other metals (e.g., Pt [8]). The Pt was found to be more active under the rich-burn conditions ($O_2/CH_4$ molar ratio <2) [9]. Although monometallic Pt catalysts were less active than the monometallic Pd catalysts under lean-burn conditions [9], some researchers [10–14] have pointed out that substituting Pt for Pd could generate a catalyst that showed enhanced catalytic activity and stability. The influence of Pt on catalytic activity of a bimetallic catalyst, however, is still a debated issue. For instance, Strobel et al. [15] investigated the combustion of methane over the supported Pd–Pt catalysts with different amounts of Pt and Pd, and observed a positive effect on catalytic performance over the supported Pd–Pt catalysts with smaller Pt amounts, but a negative effect on catalytic activity was observed over the supported Pd–Pt catalysts with higher Pt loadings. Such a phenomenon was also reported by Persson et al. [16], who claimed

* Corresponding authors.
*E-mail addresses:* yxliu@bjut.edu.cn (Y. Liu), jgdeng@bjut.edu.cn (J. Deng), hxdai@bjut.edu.cn (H. Dai).

http://dx.doi.org/10.1016/j.mcat.2017.09.002
2468-8231/

that the Pt could act either as a promoter or as an inhibitor for methane combustion. Castellazzi et al. [13] attributed this result to the extent of PdO formation, the strength of the metal–support interaction, and the stabilization of metallic $Pd^0$.

Recently, the materials consisting of mesoporous networks have been found to be highly active for some reactions. These porous materials possess large specific surface areas, high structural stability, and good catalytic durability due to their nanoscale skeletons and inter-connected hollow channels that are favorable for easy mass transfer and high electron conductivity [17,18]. In the past years, porous noble metal nanostructures have gained enormous attention [19–24]. For example, the 3D porous architecture could not only maximize the availability of electron transfer within nanosized surface but also provide better mass transfer of reactants to the catalyst [18]. Xu and coworkers [22,24] conducted a systematic investigation on the catalytic properties of nanoporous gold, and found that the porous Au catalysts performed well in the oxidation of CO.

It has been generally accepted that the metal–support interaction plays an important role in improving the catalytic activity of a supported noble metal catalyst. In order to leave out the effect of the metal-support interaction, only noble metals can be used as catalyst to investigate their catalytic performance and hence clarify the active sites. Up to now, however, there have been no reports on the preparation and catalytic applications of mesoporous $Pd_xPt$ alloys for methane combustion. In the present work, we used the mesoporous silica (KIT-6) as hard template to fabricate the mesoporous Pd, Pt and $Pd_xPt$ alloys, characterized their physicochemical properties, and evaluated their catalytic performance for methane combustion. It is found that the $Pd_xPt$ alloys showed much better catalytic activity than the monometallic Pd or Pt.

## 2. Experimental

### 2.1. Catalyst preparation

Ordered mesoporous silica (KIT-6) was synthesized under the hydrothermal conditions at 100 °C for 24 h according to the procedure of the previous literature [25]. As confirmed by the small-angle X-ray diffraction pattern (Fig. S1) and transmission electron microscopic image (Fig. S2), the as-synthesized KIT-6 template possessed an ordered mesoporous architecture with an average pore size of 6.8 nm. The mesoporous bimetallic $Pd_xPt$ alloys were prepared using the nanocasting method with KIT-6 as hard template. The typical preparation procedures are as follows: 1.00 g of KIT-6 was added to 40 mL of hexane at room temperature (RT). After being vigorously stirred for 30 min and sonication for another 30 min, a mixture of $H_2PdCl_4$ (0.56 mol/L) and $H_2PtCl_6$ (0.56 mol/L) aqueous solution was then added dropwise under stirring. The ratio of the volume of precursor aqueous solution to the pore volume of silica was 1.0. The hexane solution was sonicated for 1 h. After removing the excessive solution, the obtained brown composite was dried at 120 °C for 24 h. Such an impregnation process was repeated several times to gain a high noble metal incorporation (30–45 wt%) into the mesopores of the KIT-6. After being dried at 120 °C for 24 h, the resulting powders were placed into a three-neck flask at the ambient temperature for 30 min under the protection of $N_2$. Then, a $NaBH_4$ aqueous solution (0.30 mol/L) was added to reduce the $H_2PdCl_4$ and $H_2PtCl_6$ precursors ($NaBH_4$/nobel metal molar ratio = 10.00:1.00). Until no $H_2$ was released, the black powders were centrifuged and the KIT-6 template was removed using a hydrofluoric acid aqueous solution (10 wt%). After being washed five times with 250 mL of deionized water (50 mL for each time), the sample was dried at 120 °C overnight, and calcined in air at a ramp of 1 °C/min from RT to 400 °C and kept at this temperature for 2 h. By adjusting the molar ratios of $H_2PdCl_4$ and $H_2PtCl_6$, the $Pd_xPt$ samples with different Pd/Pt molar ratios ($x$) were obtained. For comparison proposes, single metal Pd or Pt was also fabricated using the above method. The nominal $x$ value was 9.00, 2.33, 1.00, and 0.43, respectively. The real noble metal contents of the samples were determined by the inductively coupled plasma atomic emission spectroscopic (ICP–AES) technique.

### 2.2. Catalyst characterization

Physicochemical Properties of the Pd, $Pd_xPt$, and Pt samples were characterized by means of techniques, such as ICP–AES, X-ray diffraction (XRD), transmission electron microscopy (TEM), high-angle annular dark-field-scanning transmission electron microscopic (HAADF–STEM) and element mapping, $N_2$ adsorption-desorption (BET), X-ray photoelectron spectroscopy, CO temperature-programmed reduction (CO-TPR), $O_2$ temperature-programmed desorption ($O_2$-TPD), $CH_4$ temperature-programmed desorption ($CH_4$-TPD), and Fourier transform infrared (FT–IR) spectroscopy. The detailed characterization procedures can be seen in the Supplementary material.

### 2.3. Catalytic activity evaluation

Catalytic activities of the samples for methane combustion were evaluated in a continuous flow fixed-bed quartz tube microreactor. The reactant mixture was composed of 2.5 vol% $CH_4$ + 20 vol% $O_2$ + 77.5 vol% $N_2$ (balance), and the space velocity (SV) was ca. 100,000 mL/(g h). All of the activity data were collected when the combustion of methane reached a steady state at a given temperature. Catalytic activities of the samples were evaluated using the temperatures ($T_{10\%}$, $T_{50\%}$, and $T_{90\%}$) required for achieving methane conversions of 10, 50, and 90%, respectively. The detailed activity evaluation procedures are put in the Supplementary material.

**Table 1**
BET surface areas, average pore sizes, pore volumes, average noble metal particle sizes ($D$), real Pd or Pt contents, and real Pd/Pt molar ratios of the samples.

| Nominal sample | Real sample | BET surface area ($m^2$/g) | Average pore size (nm) | Pore volume ($cm^3$/g) | XRD result | | ICP–AES result | | |
|---|---|---|---|---|---|---|---|---|---|
| | | | | | Crystal phase | $D$[a] (nm) | Real Pd content[b] (wt%) | Real Pt content[b] (wt%) | Real Pd/Pt molar ratio[b] (mol/mol) |
| Pd | Pd | 30.2 | 19.8 | 0.137 | Cubic | 9.4 | 100 | – | – |
| $Pd_9Pt_1$ | $Pd_{8.52}Pt$ | 25.5 | 18.1 | 0.131 | Cubic | 7.9 | 82.3 | 17.7 | 8.52 |
| $Pd_7Pt_3$ | $Pd_{2.41}Pt$ | 31.9 | 15.6 | 0.142 | Cubic | 7.1 | 56.8 | 43.2 | 2.41 |
| $Pd_5Pt_5$ | $Pd_{0.99}Pt$ | 29.2 | 14.9 | 0.149 | Cubic | 7.2 | 35.1 | 64.9 | 0.99 |
| $Pd_3Pt_7$ | $Pd_{0.43}Pt$ | 29.6 | 14.4 | 0.147 | Cubic | 7.4 | 18.9 | 81.1 | 0.43 |
| Pt | Pt | 31.1 | 13.7 | 0.123 | Cubic | 6.8 | – | 100 | – |

[a] Data were calculated according to the Scherrer equation using the FWHM of the (111) line of cubic Pd or Pt.
[b] Data were determined by the ICP – AES technique.

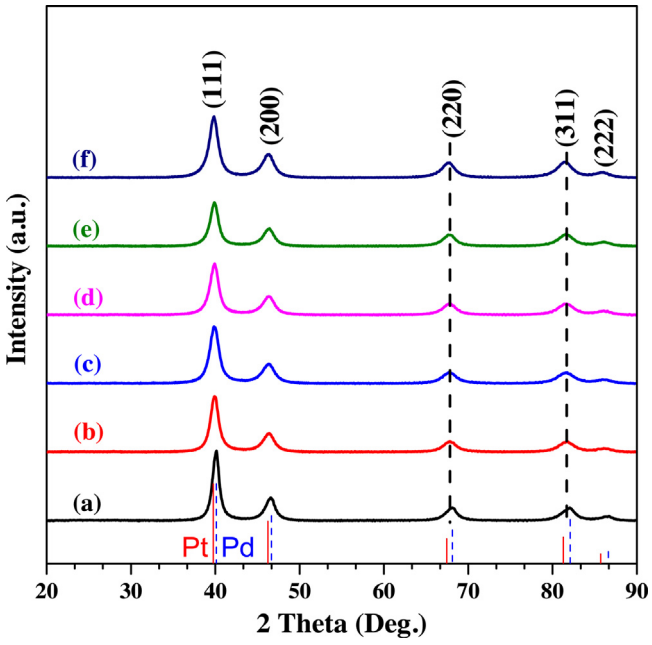


**Fig. 1.** XRD patterns of (a) Pd, (b) $Pd_{8.52}Pt$, (c) $Pd_{2.41}Pt$, (d) $Pd_{0.99}Pt$, (e) $Pd_{0.43}Pt$, and (f) Pt.

## 3. Results and discussion

### 3.1. Crystal phase composition, pore structure, and surface area

The results (Table 1) of ICP–AES investigations reveal that the real Pd/Pt molar ratios ($x$) in the $Pd_xPt$ samples were 8.52, 2.41, 0.99, and 0.43, respectively, corresponding to the nominal Pd/Pt molar ratios of 9.00, 2.33, 1.00, and 0.43. Obviously, the real and nominal Pd/Pt molar ratios in the $Pd_xPt$ samples were rather close, indicating that the preparation method was quite effective.

Fig. 1 shows the XRD patterns of the Pd, Pt, and $Pd_xPt$ samples. Compared to the XRD patterns of the standard Pd (JCPDS PDF# 46-1043) and Pt (JCPDS PDF# 04-0802) samples, one can realize that the diffraction peaks $2\theta = 40^\circ$, $46^\circ$, $68^\circ$, $82^\circ$, and $86^\circ$ were assigned to the (111), (200), (220), (311) and (222) crystal planes, and could be indexed to the face-centered cubic crystal structure. It can be also observed that the diffraction peak due to the (111) crystal plane gradually shifted to a lower $2\theta$ with increasing the Pt content in the $Pd_xPt$ samples, and it located at the $2\theta$ between those of the Pd(111) and Pt(111) crystal planes, indicating that an alloy was formed in the $Pd_xPt$ samples. Since the Pd and Pt samples were of a face-centered cubic structure, the diffraction patterns of the $Pd_xPt$ alloys were similar to those of the pure Pd or Pt sample [26]. The average grain sizes (Table 1) could be estimated according to the Scherrer equation ($D = 0.89\lambda/(\beta\cos\theta)$, where $\lambda$ is the X-ray wavelength, $\beta$ is the full width at half maximum (FWHM) of the (111) plane of the sample, and $\theta$ is the corresponding diffraction angle). It is seen that the calculated grain sizes of the Pd, Pt, and $Pd_xPt$ samples were in the range of 6.8–9.4 nm.

Fig. 2 shows the TEM images of the as-obtained noble metal samples. The distinct color contrast between the dark skeletons and bright background region suggests the formation of a three-dimensional continuous network structure with interconnected hollow voids in each of the noble metal sample. In other words, a mesoporous architecture was generated in these samples. From the SAED patterns (insets of Fig. 2) of the samples, one can see several bright diffraction rings, which was indicative of formation of polycrystalline noble metals. The wall thickness of the mesopores in the samples was 7–10 nm. Furthermore, the HAADF–STEM and element analysis images (Fig. 3) of the typical $Pd_{2.41}Pt$ sample clearly show that the distributions of Pd and Pt in the $Pd_{2.41}Pt$ sample throughout the entire domain were highly uniform. That is to say, the Pd and Pt was present in the form of an alloy in the $Pd_{2.41}Pt$ sample, in good agreement with the XRD results.

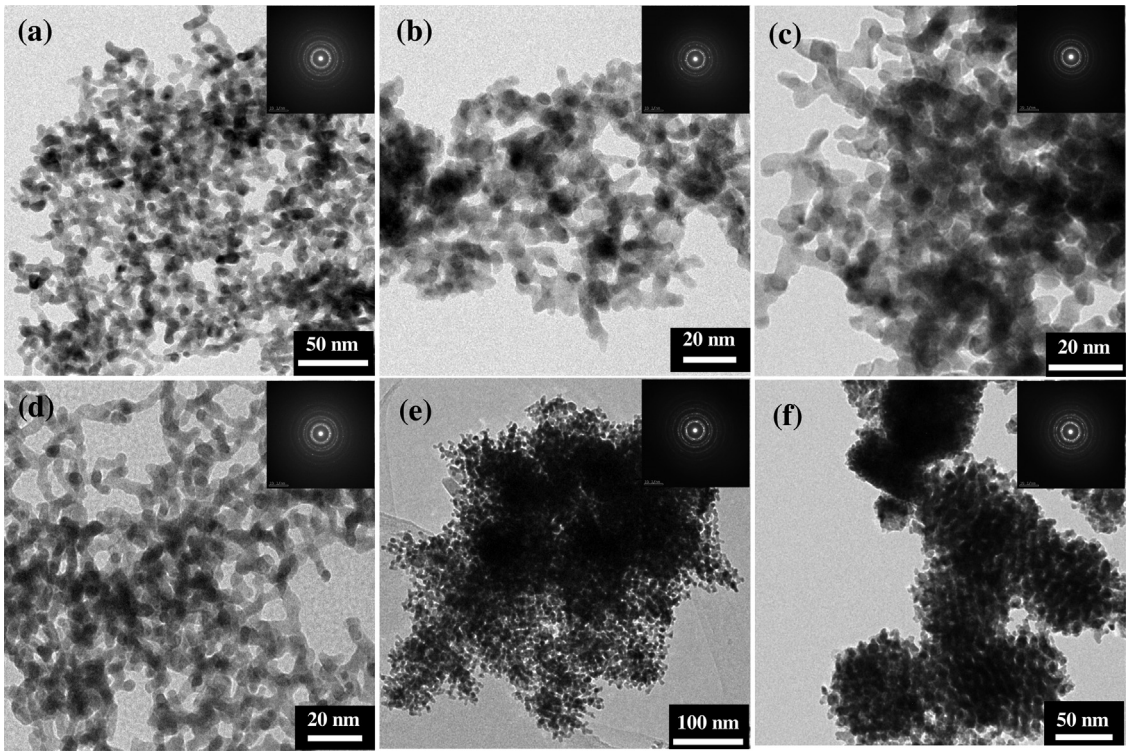


**Fig. 2.** TEM images of (a) Pd, (b) $Pd_{8.52}Pt$, (c) $Pd_{2.41}Pt$, (d) $Pd_{0.99}Pt$, (e) $Pd_{0.43}Pt$, and (f) Pt.

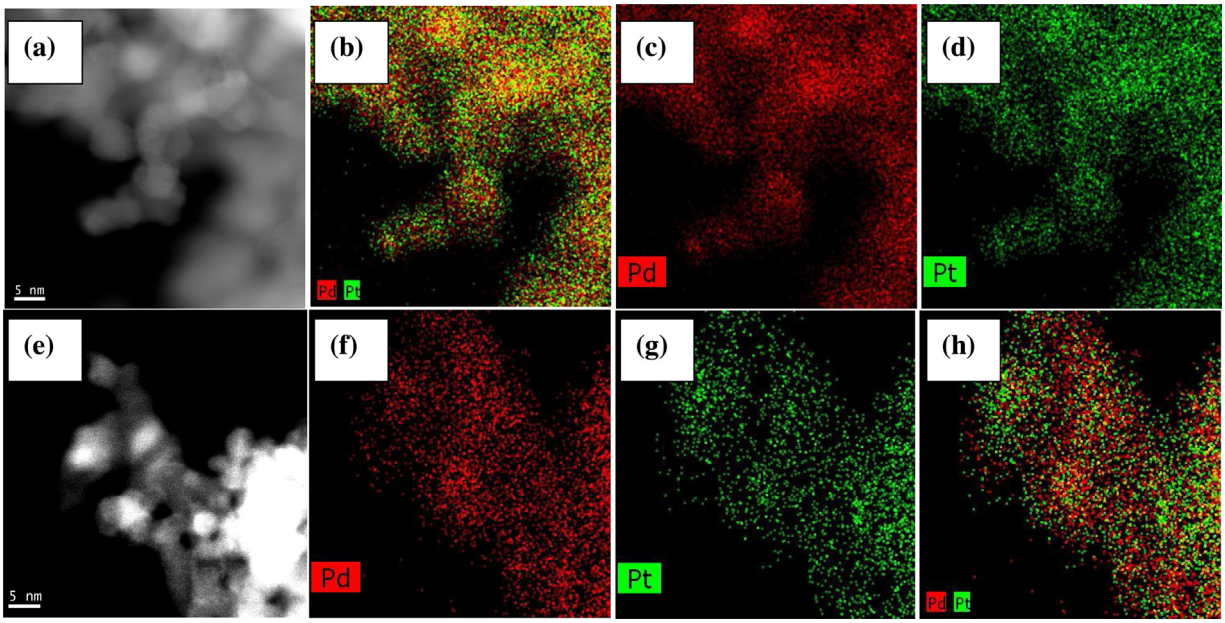


**Fig. 3.** (a and e) HAADF-STEM images and (b–d, f–h) elemental mapping of the $Pd_{2.41}Pt$ sample in different regions.

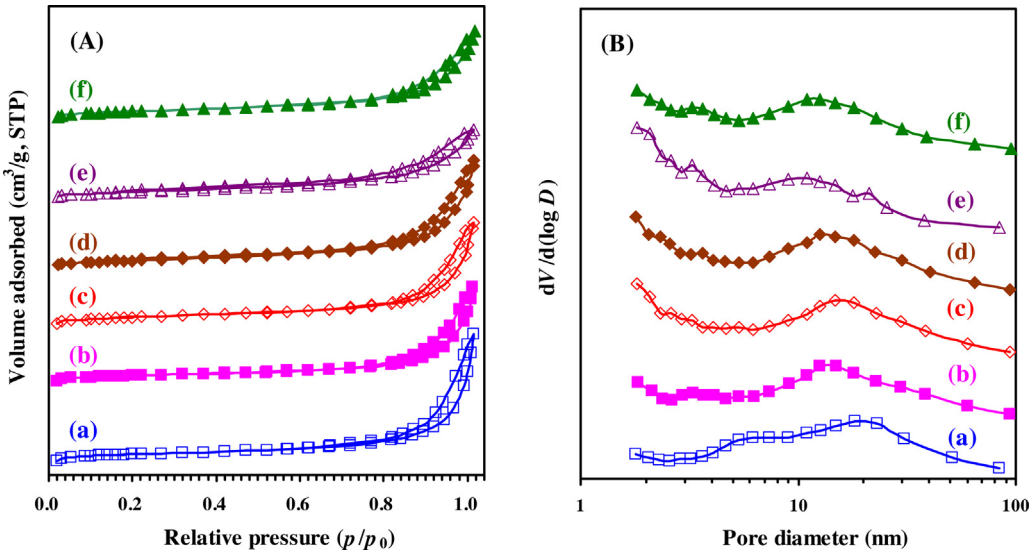


**Fig. 4.** (A) Nitrogen adsorption–desorption isotherms and (B) pore-size distributions of (a) Pd, (b) $Pd_{8.52}Pt$, (c) $Pd_{2.41}Pt$, (d) $Pd_{0.99}Pt$, (e) $Pd_{0.43}Pt$, and (f) Pt.

Fig. 4 shows the $N_2$ adsorption–desorption isotherms and pore-size distributions of the mesoporous Pd, Pt, and $Pd_xPt$ samples, and their BET surface areas, average pore sizes, and pore volumes are summarized in Table 1. It is observed from Fig. 4A that each sample displayed a type II isotherm with a H2 hysteresis loop in the relative pressure ($p/p_0$) of 0.8–1.0. The H2 hysteresis loop (which showed a large uptake) was related to the distortion of mesopores [27]. The formation of mesopores in these noble metal samples is also confirmed by their pore-size distributions (Fig. 4B). The pore sizes were in the range of 5–30 nm, with the average pore sizes being 13.7–19.8 nm (Table 1). The BET surface areas and pore volumes of the noble metal samples were in the ranges of 25.5–31.9 $m^2/g$ and 0.123–0.149 $cm^3/g$, respectively.

### 3.2. Surface elemental composition and metal oxidation state

XPS is an effective technique to determine the surface elemental compositions and metal states of a catalyst. The Pd 3d XPS spectrum is composed of the Pd $3d_{5/2}$–Pd $3d_{3/2}$ spin-orbit doublets, and the binding energy (BE) of the spin-orbital splitting is 5.26 eV. For PdO, the BE of Pd $3d_{5/2}$ was 336.6–337.7 eV [28]. Fig. 5 illustrates the Pd 3d and Pt 4f XPS spectra of the samples and their surface element compositions are summarized in Table 2. Compared to the bulk element compositions obtained from the ICP–AES technique, the surface Pd/Pt molar ratios (Table 2) of the $Pd_xPt$ samples were higher (except for the $Pd_{0.99}Pt$ sample). By using the curve-fitting approach, each Pd 3d spectrum could be decomposed into four components at BE = 335.5, 337.3, 340.7, and 342.6 eV (Fig. 5A): the components at BE = 335.5 and 340.7 eV were attributed to the surface $Pd^0$ species, whereas the ones at BE = 337.3 and 342.6 eV were assigned to the surface $Pd^{2+}$ species [28–32]. It can be clearly observed that with increasing the Pt content in the $Pd_xPt$ samples, the surface $Pd^{2+}$ content decreased but the surface $Pd^0$ content increased, indicating that the partial amount of surface PdO was reduced by the Pt. That is to say, the surface $Pd^{2+}$ concentration could be modified by the doping of Pt. Similarly, the Pt 4f XPS

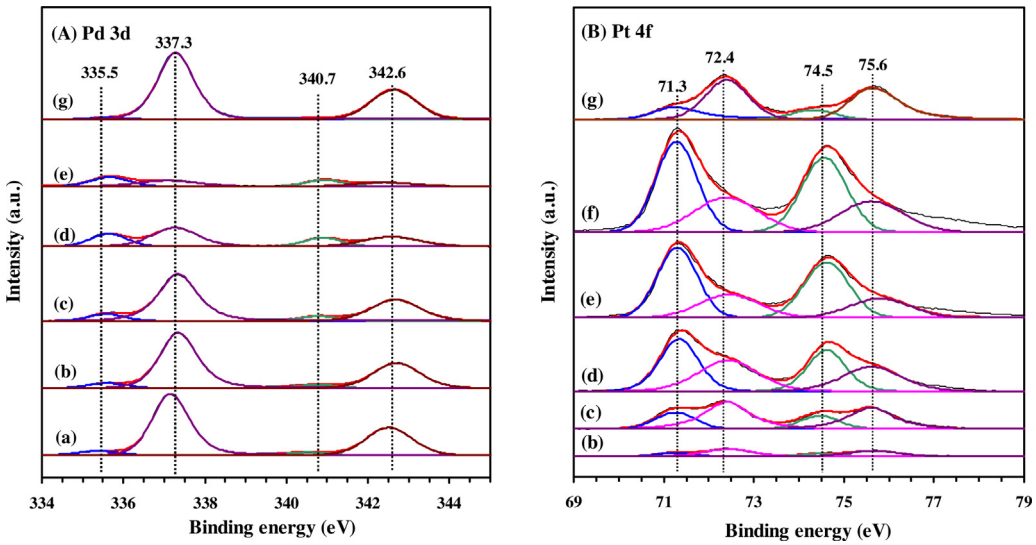


**Fig. 5.** (A) Pd 3d and (B) Pt 4f XPS spectra of (a) Pd, (b) $Pd_{8.52}Pt$, (c) $Pd_{2.41}Pt$, (d) $Pd_{0.99}Pt$, (e) $Pd_{0.43}Pt$, (f) Pt, and (g) used $Pd_{2.41}Pt$.

**Table 2**
Surface element compositions, catalytic activities, TOFs, and specific reaction rates at 280 °C and SV = 100,000 mL/(g h) of the samples.

| Sample | Surface element composition | | | Catalytic activity | | | Methane combustion at 280 °C | | | |
|---|---|---|---|---|---|---|---|---|---|---|
| | $Pd^{2+}/Pd^0$ molar ratio | $Pt^{4+}/Pt^0$ molar ratio | Pd/Pt molar ratio | $T_{10\%}$ (°C) | $T_{50\%}$ (°C) | $T_{90\%}$ (°C) | $TOF_{Pd}$[b] ($\times10^{-3}$ $s^{-1}$) | $TOF_{Pt}$[b] ($\times10^{-3}$ $s^{-1}$) | $TOF_{Pd+Pt}$[b] ($\times10^{-3}$ $s^{-1}$) | Specific reaction rate ($\mu$mol/($g_{cat}$ s)) |
| Pd | 12.75 | – | – | 313 | 350 | 368 | 0.11 | – | – | 1.06 |
| $Pd_{8.52}Pt$ | 11.10 | 2.78 | 12.66 | 297 | 338 | 351 | 0.21 | 1.92 | 0.19 | 1.67 |
| $Pd_{2.41}Pt$ | 7.57 | 2.12 | 2.82 | 272 | 303 | 322 | 0.85 | 1.98 | 0.59 | 4.46 |
| $Pd_{0.99}Pt$ | 1.86 | 0.90 | 0.90 | 292 | 322 | 338 | 0.45 | 0.45 | 0.22 | 1.49 |
| $Pd_{0.43}Pt$ | 1.03 | 0.48 | 0.46 | 292 | 328 | 348 | 0.95 | 0.41 | 0.28 | 1.69 |
| Pt | – | 0.58 | – | 282 | 372 | 506 | – | 0.53 | – | 2.70 |
| Used $Pd_{2.41}Pt$[a] | 40.69 | 2.93 | 2.78 | 254 | 283 | 306 | – | – | – | – |

[a] Used sample after the drop and rise in reaction temperature.
[b] $TOF_{Pd}$, $TOF_{Pt}$, and $TOF_{Pd+Pt}$ were calculated according to $TOF_M = XC_0/n_M$ ($n_M$ is the molar amount of Pd, Pt or Pd + Pt in the samples, respectively).

spectrum of each sample could also be decomposed into four components (Fig. 5B): the components at BE = 71.3 and 74.5 eV were ascribed to the surface metallic Pt ($Pt^0$) species, while the ones at BE = 72.4 and 75.6 eV were due to the surface oxidized Pt ($Pt^{4+}$) species [33–35]. The surface $Pt^{4+}/Pt^0$ molar ratio decreased with increasing the Pt content in the $Pd_xPt$ samples, but that on the $Pd_{0.43}Pt$ surface was slightly lower than that on the monometallic Pd surface. Since Pt is higher than Pd in electronegativity (the Pauling electronegativity of Pt and Pd is 2.28 and 2.20, respectively) [36], a charge transfer would occur from Pd to Pt in the bimetallic catalysts via $Pt^0 + Pd^{2+} \rightarrow Pt^{4+} + Pd^0$. That is to say, Pt addition can enhance the $Pd^0$ concentration due to the strong electronic interaction between Pd and Pt. The XPS results reveal that the surface $Pd^{2+}$ concentration decreased but the surface $Pd^0$ concentration increased, which are in good agreement with the fact that Pt possesses higher electron affinity than Pd. Therefore, the doping of Pt could reduce the ability of Pd to form the PdO phase. The formation of PtPd/PdO core-shell structures has been proposed by some researchers [16,37,38]. According to the XPS results, we deduce that Pd and Pt might be oxidized on the surface after calcination of the Pd, Pt or $Pd_xPt$ sample, forming $PdO_x$, $PtO_x$ or even Pd–O–Pt bonds due to their similar electronic properties; whereas Pd–Pt metallic alloy might be generated in the bulk of $Pd_xPt$. It should be pointed out that slight shifts in BE were seen in the Pd 3d and Pt 4f XPS spectra of the $Pd_xPt$ samples, but their BE values were also similar to those reported in the literature [16,28]. The $Pd_{2.41}Pt$ sample after the drop and rise in reaction temperature was characterized by the XPS technique in order to investigate the changes in chemical state of noble metals (Fig. 5g). Obviously, the surface oxidized Pd and Pt concentrations increased after a recycle of methane combustion when the reaction temperature dropped and rose again. Such a result suggests that a higher surface PdO–$PtO_2$ species concentration would be favorable for methane combustion.

### 3.3. Reducibility

The reducibility of the Pd, Pt, and $Pd_xPt$ samples was measured by the CO-TPR technique. Fig. 6 illustrates the CO-TPR profiles of the samples. The Pd sample showed the highest amount of $CO_2$ formed at 132 °C. For the Pt sample, there were three peaks of $CO_2$ formation at 83, 280, and 345 °C, respectively. However, the $Pd_xPt$ samples displayed different reduction behaviors, depending upon their Pd/Pt molar ratios. Each of the Pt-containing bimetallic samples showed one small peak at 60–70 °C and one broad peak at 90–300 °C, confirming the formation of a Pd–Pt alloy. The adsorbed CO could reduce the oxidized Pd and/or Pt at elevated temperatures. Haneda et al. [39] studied the reducibility of the $PdPt/Al_2O_3$ samples by the CO-TPR technique, and observed a new reduction peak above 200 °C (which was ascribed to the reduction of alloyed Pd–Pt NPs) in addition to the broader reduction peaks at 100–200 °C.

However, the catalytic activity cannot be fully correlated with the result of the CO-TPR study. Castellazzi et al. [13] reported strong evidence against a direct correlation between activity and PdO reducibility in the Pt-containing catalysts. Such a lack in cor-

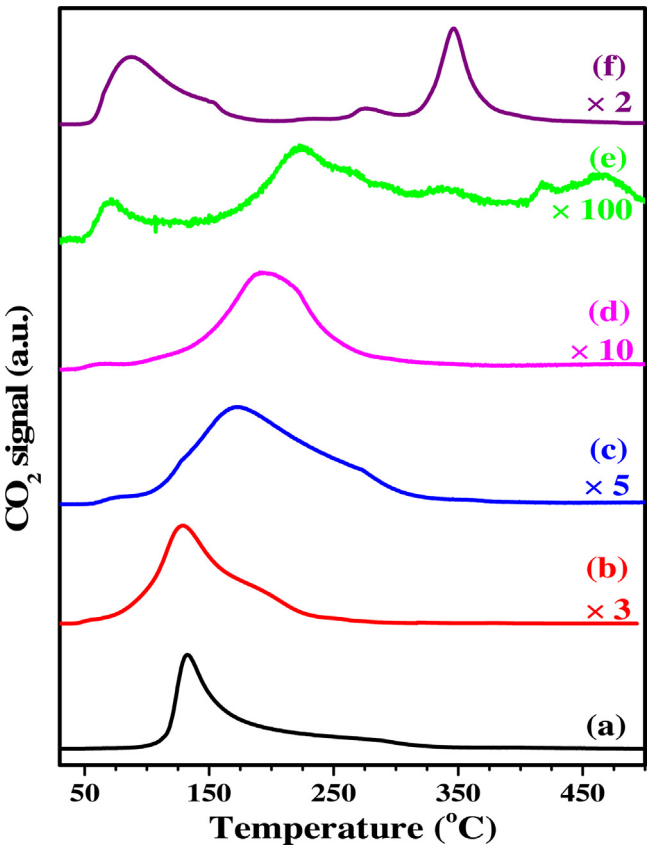


**Fig. 6.** CO–TPR profiles of (a) Pd, (b) $Pd_{8.52}Pt$, (c) $Pd_{2.41}Pt$, (d) $Pd_{0.99}Pt$, (e) $Pd_{0.43}Pt$, and (f) Pt.

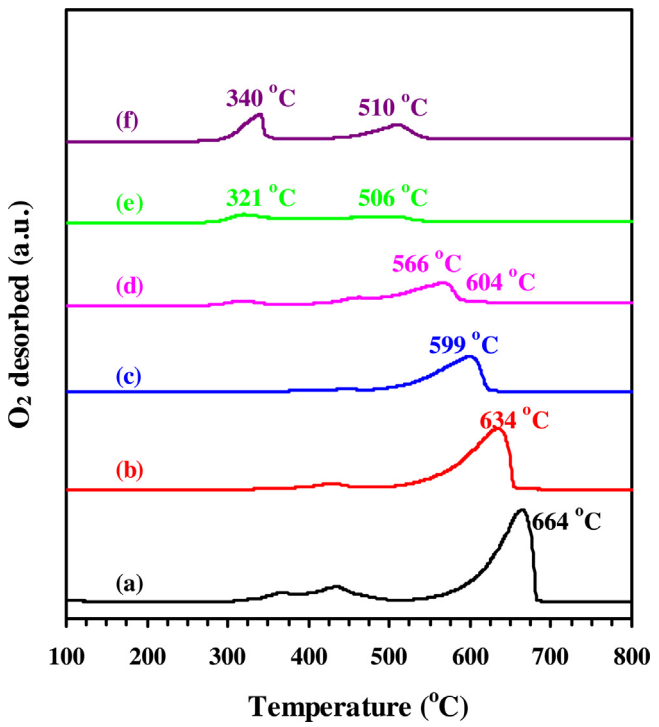


**Fig. 7.** $O_2$–TPD profiles of (a) Pd, (b) $Pd_{8.52}Pt$, (c) $Pd_{2.41}Pt$, (d) $Pd_{0.99}Pt$, (e) $Pd_{0.43}Pt$, and (f) Pt.

relation between reducibility and activity implies that the other factors rather than the surface PdO reduction could partially control the methane combustion rate over the bimetallic samples. Yashnik et al. [28] observed that a rise in the Pt share resulted in a drop in PdO amount of the $PdPt/MnLaAl_{11}O_{19}$ catalyst due to formation of the Pd–Pt alloy, and the formed Pd–Pt alloy implicitly influenced the redox and catalytic performance; when the Pt content increased, the redox properties of the bimetallic catalysts was worsen due to the rise in the share of $PtO_2$ particles. Such a mismatch between reducibility and activity suggests the contributions of the other factors for methane combustion. Therefore, we conducted the $O_2$-TPD and $CH_4$-TPD experiments to gain more clear insights to the other factors influencing the combustion of methane over the $Pd_xPt$ samples.

### 3.4. Desorption behavior

To gain a more clear insight into the effect of Pt on the redox behavior of the $Pd_xPt$ samples, we carried out the $O_2$-TPD experiments and their profiles are illustrated in Figs. 7 and S3. For all of the samples, the $O_2$ desorption peaks centered at low temperatures (300–480 °C) were due to desorption of adsorbed oxygen species (e.g., $O_2^-$, $O_2^{2-}$ or $O^-$), whereas the ones at high temperatures 500–700 °C) were due to desorption of lattice oxygen in the oxidized Pd and/or Pt (i.e., PdO and/or $PtO_2$). As shown in Fig. 7, the $O_2$-TPD profile was strongly modified by the addition of Pt to the Pd sample, and the Pd-like behavior slowly changed to the Pt-like behavior. Such observations were in good agreement with those reported in the literature [5,13,16,40]. Two main phenomena should be noticed: (i) the concentration of the adsorbed oxygen species on the samples decreased with the rise in Pt content; and (ii) when the Pt content increased, the $O_2$ desorption peaks of the samples became lower in intensity and shifted to lower temperatures, suggesting that the presence of Pt weakened the Pd–O bond strength [13,40]. The results of XPS, TPR, and $O_2$-TPD studies demonstrate formation of the $PdO_x$ and/or $PtO_x$ species, which were mainly distributed on the particle surface of each sample. We also measured the $O_2$ desorption amounts of the samples, and they decreased in the sequence of Pd (8.46 mmol/g) > $Pd_{8.52}Pt$ (6.84 mmol/g) > $Pd_{2.41}Pt$ (4.30 mmol/g) > $Pd_{0.99}Pt$ (2.94 mmol/g) > Pt (2.00 mmol/g) > $Pd_{0.43}Pt$ (1.21 mmol/g), a result due to the drop in PdO content of the samples. The decreasing PdO (i.e., increasing Pt) content was in line with the results of XPS and CO-TPR investigations. However, desorbed amounts of the adsorbed oxygen species decreased in the sequence of Pd (2.32 mmol/g) > Pt (1.42 mmol/g) > $Pd_{8.52}Pt$ (1.15 mmol/g) > $Pd_{0.43}Pt$ (1.02 mmol/g) > $Pd_{0.99}Pt$ (0.90 mmol/g) > $Pd_{2.41}Pt$ (0.64 mmol/g). Although the $Pd_{2.41}Pt$ sample exhibited a less amount of adsorbed oxygen desorption, methane combustion activity over it was higher than those over the other samples (see below). Lapisardi et al. [40] also reported the same observations, and pointed out that the doping of PdO with Pt (even in a small Pt content) could induce the Pd–Pt interactions which led to the improved catalytic activity of the Pt-doped PdO sample for methane combustion. Persson et al. [16] claimed that the metallic noble metal phase could be maintained even in an oxidizing atmosphere due to the formation of a Pd–Pt alloy in the catalysts, resulting in a better activity as compared with the monometallic Pd catalyst. Another possible reason for the higher catalytic activity might be that a more amount of $O_2$ molecules could be dissociatively adsorbed over the Pd–Pt alloys than over the PdO phase, so that the alloy provided the PdO with oxygen after reduction. The metals were much more active than the metal oxides in dissociating oxygen and the Pt metal was better than the Pd metal [41]. Hence, the superior property for $O_2$ activation of the Pd–Pt alloys might be the reason why the sample containing a lower PdO content could perform better.

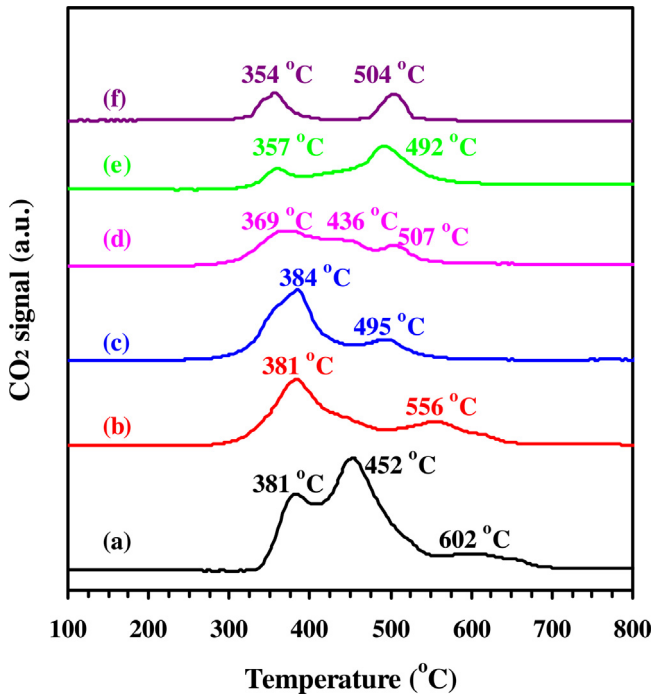


**Fig. 8.** $CH_4$–TPD profiles of (a) Pd, (b) $Pd_{8.52}Pt$, (c) $Pd_{2.41}Pt$, (d) $Pd_{0.99}Pt$, (e) $Pd_{0.43}Pt$, and (f) Pt.

It is commonly known that adsorption of reactants is a key step in heterogeneous catalysis. For methane combustion, the methane adsorption ability is possibly the key factor influencing the activity of a catalyst. $CH_4$-TPD experiments were conducted to gain insights into the activation ability of the noble metal samples. However, it should be mentioned that desorption of methane from the $Pd_xPt$ samples could be regarded as the temperature-programmed oxidation (TPO) of carbon species originated from methane [42]. As detected by the mass spectrometer, there was carbon dioxide ($m/z = 44$) signal but almost no methane ($m/z = 15$) signal from the surface of the samples. The results indicate that $CH_4$ on the catalyst surface mainly existed in chemical adsorption form and then reacted with the oxygen species, eventually desorbing as $CO_2$. As shown in the $CH_4$-TPD profiles (Fig. 8) of the samples, there were three $CO_2$ desorption peaks centered at 382, 452, and 602 °C for the monometallic Pd sample, respectively. Compared to the Pt-containing samples, the addition of Pt induced a significant effect on $CO_2$ desorption, in which $CO_2$ formation occurred at lower temperatures. That is to say, the Pt-containing samples exhibited a stronger methane activation ability than the monometallic Pd sample. This result demonstrates that Pt was beneficial for methane activation. It is generally accepted that the Pd-based catalysts perform better for methane combustion, whereas the Pt-based ones are more suitable for the oxidation of higher hydrocarbons. Burch and coworkers [43] proposed that Pt could activate the almost non-polar C–H bonds of methane via a hemolytic mechanism (dissociative adsorption of $CH_4$ at noble metal sites). Castellazzi et al. [13] also reported the dissociative adsorption of $CH_4$ on the Pt surface. According to the results of CO-TPR, $O_2$-TPD, and $CH_4$-TPD studies, the Pt sample showed lower $O_2$ and $CO_2$ desorption temperatures as compared with other samples at the low-temperature region, which might be a result possibly due to the strong dissociation ability of methane and $O_2$ molecules on the Pt surface. Therefore, the Pt sample was more active than the bimetallic samples at lower temperatures.

The $CO_2$ desorption amounts of the samples reveal important information related to the adsorption of $CH_4$. However, the decreased $CO_2$ quantity with the rise in Pt content of the $Pd_xPt$ samples were mainly due to the decreased concentration of the oxygen species. It is noticeable that for the $Pd_{2.41}Pt$ sample, the peak centered at 381 °C was nearly the same intensity as compared with that for the Pd sample, but the peak centered at 556 °C reduced dramatically in intensity. Such results confirm that the methane molecules adsorbed on the $Pd_{2.41}Pt$ surface could easily be activated and react with the adsorbed oxygen species to produce $CO_2$ and $H_2O$, a result possibly due to the strong dissociation ability of methane molecules on the Pd–Pt alloys. The results of CO-TPR, $O_2$-TPD, and $CH_4$-TPD investigations reveal that the doping of Pt to Pd gave rise to the bimetallic $Pd_xPt$ catalysts with decreased amounts of PdO species and stronger ability to active $O_2$ or $CH_4$, as compared with the pure Pd sample. Such a phenomenon might be due to the interaction between Pd and Pt, leading to the formation of a Pd–Pt alloy in $Pd_xPt$ and $PdO_x$ and $PtO_x$ species on the surface of the $Pd_xPt$ samples. Persson et al. [16] reported that the PdO amount in the sample did not influence the onset temperature of PdO decomposition, but only changed its peak intensity. Hence, the shift in temperature of CO reduction or $O_2$ desorption observed over the $Pd_xPt$ samples in the CO-TPR and $O_2$-TPD profiles was attributed to the promotion effect of Pt doping to Pd, rather than due to the lower PdO amount.

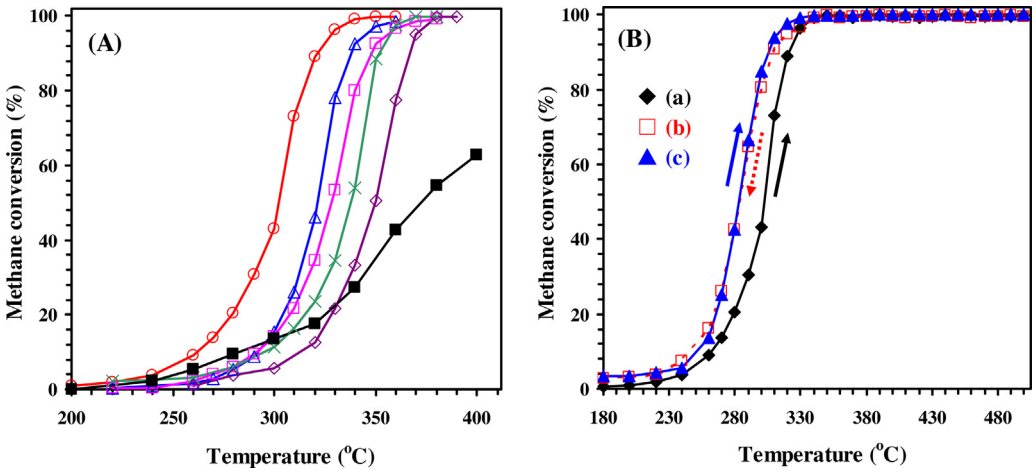


**Fig. 9.** (A) Methane conversion as a function of temperature over (◇) Pd, (×) $Pd_{8.52}Pt$, (○) $Pd_{2.41}Pt$, (△) $Pd_{0.99}Pt$, (□) $Pd_{0.43}Pt$, and (■) Pt; (B) methane conversion versus temperature over the $Pd_{2.41}Pt$ sample when the temperature (a) rose, (b) dropped, and (c) rose again at SV = 100,000 mL/(g h).

### 3.5. Catalytic performance

Fig. 9A shows the methane conversion versus temperature over the as-prepared samples at a SV of 100,000 mL/(g h). It is convenient to compare the catalytic activities of the samples using the reaction temperatures ($T_{50\%}$ and $T_{90\%}$) requiring for achieving methane conversions of 50 and 90% (Fig. 9A and Table 2), respectively. Among all of the samples, the $Pd_{2.41}Pt$ sample showed the best catalytic activity: $T_{50\%}$ = 303 °C and $T_{90\%}$ = 322 °C, which were much lower than those over the monometallic Pd ($T_{50\%}$ = 350 °C and $T_{90\%}$ = 368 °C) and Pt ($T_{50\%}$ = 372 °C and $T_{90\%}$ = 506 °C) samples. Therefore, the catalytic activity decreased in the sequence of $Pd_{2.41}Pt > Pd_{0.99}Pt > Pd_{0.43}Pt > Pd_{8.52}Pt > Pd > Pt$. It should be noted that all of the $Pd_xPt$ alloy samples outperformed the monometallic Pd or Pt sample, which was not in consistency with the results reported in the literature [15,16]. The excellent catalytic performance of the $Pd_xPt$ alloy samples might be associated with the co-existence of Pd–Pt alloy and PdO–$PtO_2$.

We measured the methane conversions over the $Pd_{2.41}Pt$ sample when the temperature rose, dropped, and rose again (Fig. 9B), respectively. Methane conversions at 180–360 °C during the temperature-dropping process were higher than those during the temperature-rising process. When the temperature rose again, however, methane conversions were rather similar to those during the temperature-dropping process. Comparing to the $T_{10\%}$, $T_{50\%}$, and $T_{90\%}$ (272, 303, and 322 °C) over the $Pd_{2.41}Pt$ sample during the first temperature-rising process, the $T_{10\%}$, $T_{50\%}$, and $T_{90\%}$ decreased to 254, 283, and 306 °C during the second temperature-rising process, respectively. Similar phenomena for methane combustion during the temperature-dropping and rising processes have been reported in the literature [4,32,44]. It is generally believed that Pd is easily oxidized into the PdO species at a certain temperature (<600 °C). Therefore, the enhancement in catalytic activity of the $Pd_{2.41}Pt$ sample might be due to generation of a more amount of the PdO species during the reaction process, which was supported by the results (much higher surface $Pd^{2+}/Pd^0$ and $Pt^{4+}/Pt^0$ molar ratios were detected on the used $Pd_{2.41}Pt$ sample (Table 2)) of the XPS investigation.

It is more accurate to use the turnover frequencies (TOFs) and specific reaction rates for evaluating the inherent catalytic activities of the samples. The $TOF_M$ ($TOF_M = XC_0/n_M$, where $X$ is the conversion at a certain temperature, $C_0$ (mol/(g s)) is the initial methane concentration per gram per second, and $n_M$ (mol) is the molar amount of Pd, Pt or Pd + Pt) and specific reaction rates can be calculated according to the activity data and amounts of Pd and Pt in the Pd, Pt, and $Pd_xPt$ samples, as summarized in Table 2. It is clearly observed that the $Pd_{2.41}Pt$ sample exhibited a relatively high $TOF_{Pd}$ ($0.85 \times 10^{-3}\ s^{-1}$), the highest $TOF_{Pt}$ ($1.98 \times 10^{-3}\ s^{-1}$), the highest $TOF_{Pd+Pt}$ ($0.59 \times 10^{-3}\ s^{-1}$), and the highest specific reaction rate (4.46 μmol/($g_{cat}$ s)) in the combustion of methane at 280 °C, a result possibly due to the interaction between Pd and Pt. Usually, it is more accurate to calculate the TOFs based on the surface atoms. However, it is well known that the surface element composition of a sample is not the same as its bulk element composition. Since the Pd/Pt molar ratios on the surface of the samples were not the same as those determined by the ICP–AES technique, it is hard to obtain the exact numbers of surface Pd and Pt atoms, which makes the calculation of the TOF values difficult. Actually, some researchers also used the total amount of the noble metal to calculate the TOF value. For example, Li et al. [45] calculated the TOFs of the PtSn/TS-1 catalysts for propane dehydrogenation according to the molar amount of Pt in the samples; Hutchings and coworkers also estimated the TOFs on the basis of the total metal loading [46–48]. Therefore, the TOFs calculated according to the molar amounts of noble metals could reflect the inherent catalytic performance of the noble metal samples.

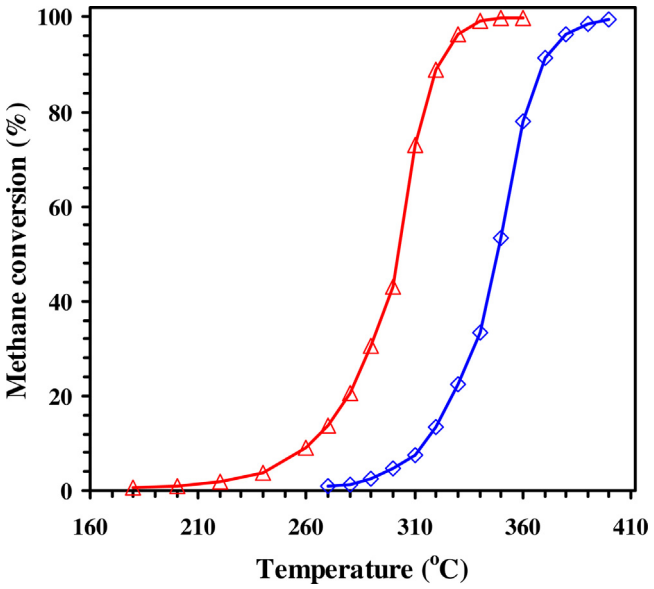


**Fig. 10.** Methane conversion versus temperature over the (△) oxidized and (◇) reduced $Pd_{2.41}Pt$ samples at SV = 100,000 mL/(g and h).

Fig. 10 shows the catalytic activities over the oxidized and reduced $Pd_{2.41}Pt$ samples for methane combustion. Obviously, methane combustion activity significantly decreased after the $Pd_{2.41}Pt$ sample was reduced in 10 vol% $H_2$–90 vol% $N_2$ (30 mL/min) at 300 °C, with the $T_{10\%}$, $T_{50\%}$, and $T_{90\%}$ increasing by 43, 42, and 46 °C, respectively. The result demonstrates that the oxidized $Pd_{2.41}Pt$ (PdO–$PtO_2$) sample in air (30 mL/min) at 400 °C was more active than the reduced $Pd_{2.41}Pt$ (metallic $Pd^0$–$Pt^0$) sample. Similar results have been reported by other researchers [2,49]. In addition, we measured the catalytic activities over the oxidized and reduced $Pd_{2.41}Pt$ samples after the "temperature rise-drop-rise" cycle, as shown in Fig. S4. The oxidized sample after the "temperature rise-drop-rise" cycle exhibited better activity than the fresh sample, but there was almost no change in activity over the reduced sample. This phenomenon could be explained by their XPS results. It is observed that the Pd/Pt molar ratio on the used $Pd_{2.41}Pt$ sample was close to that on the fresh $Pd_{2.41}Pt$ sample (Table 2), indicating no significant changes in Pd/Pt molar ratio on the surface of the fresh and used $Pd_{2.41}Pt$ samples. The concentrations of PdO and $PtO_2$, however, increased after the "temperature rise-drop-rise" cycle, resulting in an increase in methane combustion activity.

In the past decades, a number of works on methane combustion have been reported in the literature, and their catalytic activities ($T_{50\%}$ and $T_{90\%}$) over the catalysts reported in the literature and the $Pd_{2.41}Pt$ catalyst reported in the present work are summarized in Table S1. Apparently, our $Pd_{2.41}Pt$ catalyst outperformed the 1.0 wt% $Pd/Al_2O_3$ [50], 1.92 wt% $Pd/Co_3O_4$ [51], 1.1 wt% Pt/3DOM $Ce_{0.6}Zr_{0.3}Y_{0.1}O_2$ [52], 3.0 wt% AuPd/3DOM $La_{0.6}Sr_{0.4}MnO_3$ [53], 3.1 wt% Pd–2.9 wt% Pt/$LaMnAl_{11}O_{19}$ [54], 5 wt% $PdCo/Al_2O_3$ [16], and 1.0 wt% Co–1.0 wt% $Pd/Al_2O_3$ [8] catalysts.

### 3.6. Effect of water vapor, $CO_2$, and $SO_2$ on catalytic activity

Although the Pd-based catalysts are the most active materials for methane combustion [1,2,8,55], their activity stability is not good enough [11,16,55,56]. It has been reported that the supported monometallic Pt catalysts were less active than the supported monometallic Pd catalysts for methane combustion [57]. The partial substitution of Pd with Pt, however, could generate a catalyst that improve its catalytic stability for methane combustion [2,58]. Fig. 11 shows the catalytic activities versus

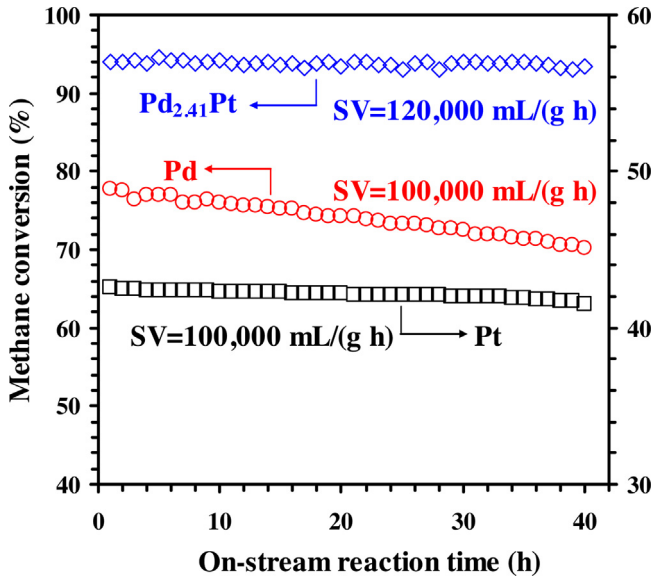


**Fig. 11.** Methane conversion versus on-stream reaction time over the Pd, $Pd_{2.41}Pt$, and Pt samples at 350 °C.

on-stream methane combustion at 350 °C over the Pd and Pt samples at SV = 100,000 mL/(g h) and over the $Pd_{2.41}Pt$ catalyst at SV = 120,000 mL/(g h). Apparently, the $Pd_{2.41}Pt$ sample exhibited the highest activity and no significant loss in activity during 40 h of on-stream reaction, indicating that the $Pd_{2.41}Pt$ sample possessed good catalytic stability. The Pt sample displayed a stability similar to that of the $Pd_{2.41}Pt$ sample, the catalytic activity was much lower over the former than that over the latter. Methane conversion over the Pd sample, however, gradually decreased from 78 to 70% within 40 h of on-stream methane combustion. We also recorded the TEM image of the used $Pd_{2.41}Pt$ sample after 40 h of on-stream methane combustion, as shown in Fig. S5. Obviously, there were no significant changes in mesostructure of the fresh and used $Pd_{2.41}Pt$ samples. Therefore, the alloying of Pd with Pt could increase the catalytic activity and stability. The good stability of the $Pd_{2.41}Pt$ sample might be associated with the fact that Pt could improve the anti-sintering ability of Pd NPs [11,15].

$H_2O$ and $CO_2$ are the products of methane combustion. It is necessary to examine the effects of $H_2O$ and $CO_2$ on catalytic activity of the typical sample. We introduced 2.5 or 5.0 vol% water vapor to the reaction system and monitored the methane conversions over the $Pd_{2.41}Pt$ sample at 310 °C and SV = 100,000 mL/(g h). As shown in Fig. 12A, methane conversion was not altered within 4 h of methane combustion in the absence of $H_2O$. In the presence of 2.5 vol% water vapor, however, methane conversion first decreased slightly (ca. 5% loss in activity) and then recovered to its original value in the absence of $H_2O$. By switching to 5.0 vol% water vapor, the catalytic activity maintained almost unchanged. After cutting off the 5.0 vol% water vapor, the catalytic activity was totally restored to that in the absence of water vapor. The results indicate that the $Pd_{2.41}Pt$ sample was catalytically stable in the presence of water vapor in a certain concentration below 5.0 vol%. As the main active phase, PdO is readily to form the $Pd(OH)_2$ species through the reaction of $PdO + H_2O \rightarrow Pd(OH)_2$ in the presence of water vapor, where the $Pd(OH)_2$ was usually regarded as an inactive phase [59]. The deactivation due to water of the Pd-based catalysts was related to the reaction temperature. Burch and coworkers [49,60] pointed out that the $PdO/Al_2O_3$ catalysts were irreversibly deactivated due to hydroxylation of PdO to inactive $Pd(OH)_2$ particles in the presence of water at a lower temperature (e.g., 300 °C), but their deactivation induced by water was insignificant at a higher temperature (e.g., 450 °C). Therefore, the stability of the $Pd_{2.41}Pt$ sample for methane combustion under the wet conditions might be related to the interaction between Pd and Pt, which not only improved the catalytic activity, but also inhibited the formation of $Pd(OH)_2$ [10–12,40]. In the case of 2.5 or 5.0 vol% $CO_2$ introduction to the reaction system over the $Pd_{2.41}Pt$ sample at 310 °C and SV = 100,000 mL/(g h), one can clearly see that the catalytic activity was durable after 20 h of methane combustion in the presence of 2.5 or 5.0 vol% $CO_2$ (Fig. 12B). Hence, $CO_2$ had no significant negative effect on catalytic activity of the $Pd_{2.41}Pt$ sample for methane combustion. Similar results have been reported in the literature [60].

To examine the effect of $SO_2$ on catalytic activity, we conducted methane combustion over the $Pd_{2.41}Pt$ sample at 310 °C and SV = 100,000 mL/(g h). As shown in Fig. 13A, methane conversion decreased from 90.0 to 31.1% after 10 h of 100 ppm $SO_2$ introduction. When the $SO_2$ was cut off, however, methane conversion slowly increased to 72.4%. This result indicates that deactivation of the $Pd_{2.41}Pt$ sample induced $SO_2$ was partially reversible. To elucidate the reason for such a deactivation of the $Pd_{2.41}Pt$ sample, we carried out the in situ DRIFT experiments, and their spectra are shown in Fig. 13B. According to the literature [32,61,62], the absorption bands of the $H_2O$, $CO_2$, and $SO_3^{2-}$ or $SO_4^{2-}$ species were at 1640 $cm^{-1}$, at 2341 and 2360 $cm^{-1}$, and at 1159 and 1045 $cm^{-1}$, respectively. It can be clearly seen from Fig. 13B that in addition to the absorption bands due to $H_2O$ and $CO_2$, there were no absorption bands assignable to the $SO_3^{2-}$ or $SO_4^{2-}$ species on the sample within 4 h of methane combustion in the absence of $SO_2$, but the absorption bands at 1159 and 1045 $cm^{-1}$ (assignable to the $SO_3^{2-}$ or $SO_4^{2-}$ species) were detected and their intensity was much

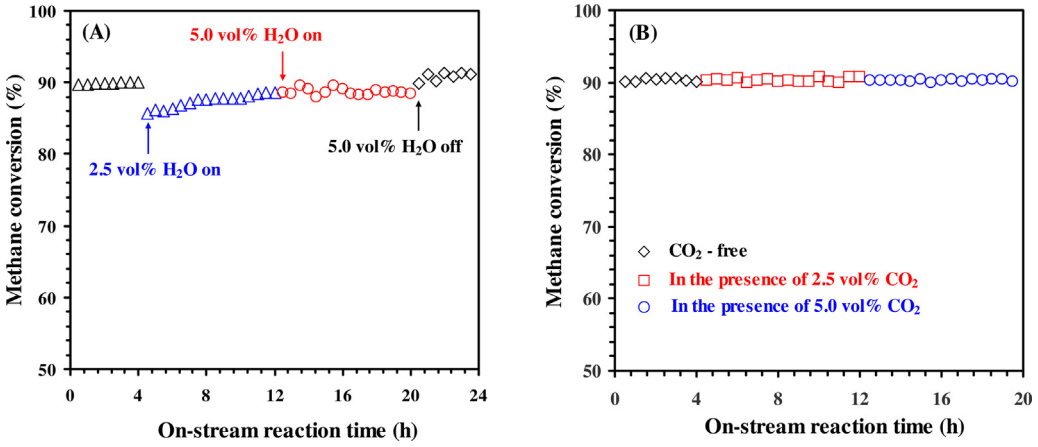


**Fig. 12.** Effects of (A) water vapor and (B) $CO_2$ on methane conversion over the $Pd_{2.41}Pt$ sample at 310 °C and SV = 100,000 mL/(g h).

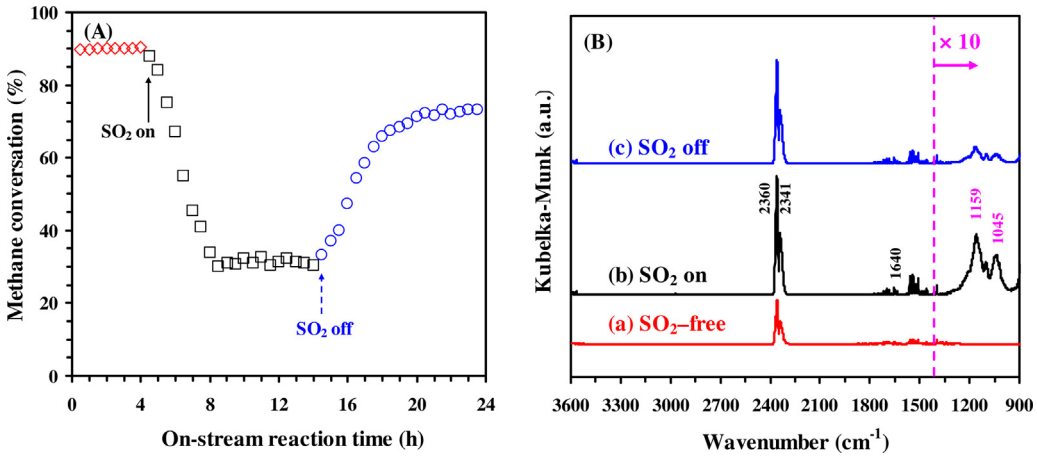


**Fig. 13.** (A) Effect of 100 ppm $SO_2$ on methane conversion over the $Pd_{2.41}Pt$ sample at 310 °C and SV = 100,000 mL/(g h), and (B) in situ DRIFT spectra of the $Pd_{2.41}Pt$ sample after (a) 4 h of methane combustion at 310 °C, (b) 10 h of methane combustion at 310 °C when 100 ppm $SO_2$ was introduced, and (c) 9 h of methane combustion at 310 °C when 100 ppm $SO_2$ was cut off.

higher after 10 h of $SO_2$ introduction than that after cutting off the $SO_2$. This result reasonably explains the partially reversible deactivation of the $Pd_{2.41}Pt$ sample induced by $SO_2$. The negative effect of $SO_2$ addition on methane combustion might be due to the attack of $SO_2$ on the PdO component in the oxidized $Pd_{2.41}Pt$ sample, which made highly active PdO transform into inactive $PdSO_3$ or $PdSO_4$. The $SO_2$, however, would have little influence on the Pd–Pt alloy, thus the partially deactivated sample still showed a methane conversion of 31.1%. After cutting off the $SO_2$, methane conversion was partially recovered (72.4%), a result possibly due to the decomposition of the weakly adsorbed $SO_2$ species. Furthermore, we activated the 100 ppm $SO_2$-treated $Pd_{2.41}Pt$ sample in a $N_2$ flow of 30 mL/min at 500 °C for 1 h, and measured its catalytic activity for methane combustion. As shown in Fig. S6, methane conversions at 310 °C over the activated $Pd_{2.41}Pt$ sample were almost recovered to the original values over the fresh $Pd_{2.41}Pt$ sample, and the catalytic activity was stable within 8 h of methane combustion.

## 4. Conclusions

The mesoporous Pd, Pt, and $Pd_xPt$ alloys could be prepared via the KIT-6-templating route. The mesoporous samples displayed a surface area of 25.5–31.9 $m^2/g$ and an average pore size of 13.7–19.8 nm. An Pd–Pt alloy was formed in each of the $Pd_xPt$ samples. The addition of Pt to Pd exerted a significant effect on the redox property of the Pd sample. The PdO–$PtO_2$ were more active than the $Pd^0$–$Pt^0$. Among all of the samples, the $Pd_{2.41}Pt$ sample showed the highest catalytic performance for methane combustion (at SV = 100,000 mL/(g h), $T_{10\%}$ = 272 °C, $T_{50\%}$ = 303 °C, and $T_{90\%}$ = 322 °C; at 280 °C, $TOF_{Pd} = 0.85 \times 10^{-3}\ s^{-1}$, $TOF_{Pt} = 1.98 \times 10^{-3}\ s^{-1}$, $TOF_{Pd+Pt} = 0.59 \times 10^{-3}\ s^{-1}$, and specific reaction rate = 4.46 μmol/($g_{cat}$ s)). The deactivation of the $Pd_{2.41}Pt$ sample induced by 2.5–5.0 vol% $CO_2$ or $H_2O$ addition was reversible, but its deactivation due to 100 ppm $SO_2$ introduction was irreversible. It is concluded that the good mesoporous structure, Pd–Pt alloy and PdO–$PtO_2$ coexistence, and good methane and oxygen activation ability were responsible for the excellent catalytic performance of the $Pd_{2.41}Pt$ sample.

## Acknowledgments

This work was supported by the NSF of China (21377008 and 21677004) and National High Technology Research and Development Program ("863" Program) of China (2015AA034603).

## Appendix A. Supplementary data

Supplementary data associated with this article can be found, in the online version, at http://dx.doi.org/10.1016/j.mcat.2017.09.002.

## References

[1] J. Xu, L. Ouyang, W. Mao, X.J. Yang, X.C. Xu, J.J. Su, T.Z. Zhuang, H. Li, Y.F. Han, ACS Catal. 2 (2012) 261–269.
[2] P. Gélin, M. Primet, Appl. Catal. B 39 (2002) 1–37.
[3] N.M. Kinnunen, J.T. Hirvi, T. Venäläinen, M. Suvanto, T.A. Pakkanen, Appl. Catal. A 397 (2011) 54–61.
[4] M. Cargnello, J.J. Delgado Jaén, J.C. Hernández Garrido, K. Bakhmutsky, T. Montini, J.J. Calvino Gámez, R.J. Gorte, P. Fornasiero, Science 337 (2012) 713–717.
[5] N. Sadokhina, G. Smedler, U. Nylén, M. Olofsson, L. Olsson, Appl. Catal. B 200 (2017) 351–360.
[6] J. Nilsson, P. Carlsson, S. Fouladvand, N.M. Martin, J. Gustafson, M.A. Newton, E. Lundgren, H. Gronbeck, M. Sköglundh, ACS Catal. 5 (2015) 2481–2489.
[7] D.N. Gao, C.X. Zhang, S. Wang, Z.S. Yuan, S.D. Wang, Catal. Commun. 9 (2008) 2583–2587.
[8] K. Persson, A. Ersson, K. Jansson, N. Iverlund, S.G. Järås, J. Catal. 231 (2005) 139–150.
[9] R. Burch, P.K. Loader, Appl. Catal. B 1–2 (1994) 149–164.
[10] H. Yamamoto, H. Uchida, Catal. Today 45 (1998) 147–151.
[11] K. Narui, H. Yata, K. Furuta, A. Nishida, Y. Kohtoku, T. Matsuzaki, Appl. Catal. A 179 (1999) 165–173.
[12] N.M. Kinnunen, J.T. Hirvi, M. Suvanto, T.A. Pakkanen, J. Mol. Catal. A 356 (2012) 20–28.
[13] P. Castellazzi, G. Groppi, P. Forzatti, Appl. Catal. B 95 (2010) 303–311.
[14] G. Corro, C. Cano, J.L.G. Fierro, J. Mol. Catal. A 315 (2010) 35–42.
[15] R. Strobel, J. Grunwaldt, A. Camenzind, S.E. Pratsinis, A. Baiker, Catal. Lett. 104 (2005) 9–16.
[16] K. Persson, A. Ersson, K. Jansson, J.L.G. Fierro, S.G. Järås, J. Catal. 243 (2006) 14–24.
[17] J.T. Zhang, C.M. Li, Chem. Soc. Rev. 41 (2012) 7016–7031.
[18] C.Z. Zhu, D. Du, A. Eychmüller, Y.H. Lin, Chem. Rev. 115 (2015) 8896–8943.
[19] X.F. Zhang, P.F. Guan, L. Malic, M. Trudeau, F. Rosei, T. Veres, J. Mater. Chem. A 3 (2015) 2050–2056.
[20] Y. Wang, N. Su, L. Ye, Y.H. Ren, X.Y. Chen, Y.J. Du, Z.H. Li, B. Yue, S.C.E. Tsang, Q. Chen, H.Y. He, J. Catal. 313 (2014) 113–126.
[21] H.J. Wang, H.Y. Jeong, M. Imura, L. Wang, L. Radhakrishnan, N. Fujita, T. Castle, O. Terasaki, Y. Yamauchi, J. Am. Chem. Soc. 133 (2011) 14526–14529.
[22] C.X. Xu, X.H. Xu, J.X. Su, Y. Ding, J. Catal. 252 (2007) 243–248.
[23] A. Saramat, P. Thormählen, M. Skoglundh, G.S. Attard, A.E.C. Palmqvist, J. Catal. 253 (2008) 253–260.
[24] H.M. Duan, C.X. Xu, J. Catal. 332 (2015) 31–37.
[25] F. Kleitz, S.H. Choi, R. Ryoo, Chem. Commun. (2003) 2136–2137.
[26] C.X. Xu, Q. Hao, H.M. Duan, J. Mater. Chem. A 2 (2014) 8875–8880.
[27] C.Z. Zhu, Q.R. Shi, S.F. Fu, J.H. Song, H.B. Xia, D. Du, Y.H. Lin, Adv. Mater. 28 (2016) 8779–8783.
[28] S.A. Yashnik, Y.A. Chesalov, A.V. Ishchenko, V.V. Kaichev, Z.R. Ismagilov, Appl. Catal. B 204 (2017) 89–106.
[29] K.R. Priolkar, P. Bera, P.R. Sarode, M.S. Hegde, S. Emura, R. Kumashiro, N.P. Lalla, Chem. Mater. 14 (2002) 2120–2128.

[30] S.H. Xie, J.G. Deng, S.M. Zang, H.G. Yang, G.S. Guo, H. Arandiyan, H.X. Dai, J. Catal. 322 (2015) 38–48.
[31] M. Brun, A. Berthet, J.C. Bertolini, J. Electron Spectrosc. 104 (1999) 55–60.
[32] S.H. Xie, J.G. Deng, S.M. Zang, Z.H. Zhang, H. Arandiyan, H.X. Dai, Environ. Sci. Technol. 51 (2017) 2271–2279.
[33] P. Bera, K.C. Patil, V. Jayaram, G.N. Subbanna, M.S. Hegde, J. Catal. 196 (2000) 293–301.
[34] M.Y. Mao, H.Q. Lv, Y.Z. Li, Y. Yang, M. Zeng, N. Li, X.J. Zhao, ACS Catal. 6 (2016) 418–427.
[35] H. Arandiyan, H.X. Dai, K.M. Ji, H.Y. Sun, J.H. Li, ACS Catal. 5 (2015) 1781–1793.
[36] J. Xu, L. Ouyang, G.J. Da, Q.Q. Song, X.J. Yang, Y.F. Han, J. Catal. 285 (2012) 74–82.
[37] A. Morlang, U. Neuhausen, K.V. Klementiev, Appl. Catal. B 60 (2005) 191–199.
[38] N.M. Martin, J. Nilsson, M. Skoglundh, E.C. Adams, X. Wang, P. Velin, G. Smedler, A. Raj, D. Thompsett, H.H. Brongersma, T. Grehl, G. Agostini, O. Mathon, S. Carlson, K. Nore, F.J. Martinezcasado, Z. Matej, O. Balmes, P. Carlsson, J. Phys. Chem. C 120 (2016) 28009–28020.
[39] M. Haneda, K. Suzuki, M. Sasaki, H. Hamada, M. Ozawa, Appl. Catal. A 475 (2014) 109–115.
[40] G. Lapisardi, L. Urfels, P. Gélin, M. Primet, A. Kaddouri, E. Garbowski, S. Toppi, E. Tena, Catal. Today 117 (2006) 564–568.
[41] S. Bedrane, C. Descorme, D. Duprez, Appl. Catal. A 289 (2005) 90–96.
[42] J.R. Paredes, E. Díaz, F.V. Díez, S. Ordóñez, Energy Fuel 23 (2009) 86–93.
[43] R. Burch, D.J. Crittle, M.J. Hayes, Catal. Today 47 (1999) 229–234.
[44] C. Chen, Y.H. Yeh, M. Cargnello, C.B. Murray, P. Fornasiero, R.J. Gorte, ACS Catal. 4 (2014) 3902–3909.
[45] J.C. Li, J.M. Li, Z. Zhao, X.Q. Fan, J. Liu, Y.C. Wei, A.J. Duan, Z.A. Xie, Q.L. Liu, J. Catal. 352 (2017) 361–370.
[46] L. Kesavan, R. Tiruvalam, M.H.A. Rahim, M.I.B. Saiman, D.I. Enache, R.L. Jenkins, N. Dimitratos, J.A. Lopez-Sanchez, S.H. Taylor, D.W. Knight, C.J. Kiely, G.J. Hutchings, Science 331 (2011) 195–199.
[47] M.I.B. Saiman, G.L. Brett, R. Tiruvalam, M.M. Forde, K. Sharples, A. Thetford, R.L. Jenkins, N. Dimitratos, J.A. Lopez-Sanchez, D.M. Murphy, D. Bethell, D.J. Willock, S.H. Taylor, D.W. Knight, C.J. Kiely, G.J. Hutchings, Angew. Chem. Int. Ed. 51 (2012) 5981–5985.
[48] G.T. Whiting, S.A. Kondrat, C. Hammond, N. Dimitratos, Q. He, D.J. Morgan, N.F. Dummer, J.K. Bartley, C.J. Kiely, S.H. Taylor, G.J. Hutchings, ACS Catal. 5 (2015) 637–644.
[49] R. Burch, F.J. Urbano, Appl. Catal. A 124 (1995) 121–138.
[50] W.R. Schwartz, D. Ciuparu, L.D. Pfefferle, J. Phys. Chem. C 116 (2012) 8587–8593.
[51] M.T. Makhlouf, B.M. Abu-Zied, T.H. Mansoure, J. Nanopart. 2013 (2013) 384350.
[52] H. Arandiyan, H.X. Dai, K.M. Ji, H.Y. Sun, J.H. Li, ACS Catal. 5 (2015) 1781–1793.
[53] K. Sasaki, O. Tanaike, H. Konno, Can Miner. 36 (1998) 1225–1235.
[54] Y. Wang, H. Arandiyan, J. Scott, M. Akia, H.X. Dai, J.G. Deng, K. Aguey-Zinsou, R. Amal, ACS Catal. 6 (2016) 6935–6947.
[55] A. Ersson, H. Kušar, R. Carroni, T. Griffin, S. Järås, Catal. Today 83 (2003) 265–277.
[56] K. Persson, K. Jansson, S.G. Järås, J. Catal. 245 (2007) 401–414.
[57] M. Lyubovsky, L.L. Smith, M. Castaldi, H. Karim, B. Nentwick, S. Etemad, R. LaPierre, W.C. Pfefferle, Catal. Today 83 (2003) 71–84.
[58] Y. Ozawa, Y. Tochihara, A. Watanabe, M. Nagai, S. Omi, Appl. Catal. A 259 (2004) 1–7.
[59] W.R. Schwartz, L.D. Pfefferle, J. Phys. Chem. C 116 (2012) 8571–8578.
[60] R. Burch, F.J. Urbano, P.K. Loader, Appl. Catal. A 123 (1995) 173–184.
[61] W.R. Schwartz, D. Ciuparu, L.D. Pfefferle, J. Phys. Chem. C 116 (2012) 8587–8593.
[62] Z.X. Wu, J.G. Deng, Y.X. Liu, S.H. Xie, Y. Jiang, X.T. Zhao, J. Yang, H. Arandiyan, G.S. Guo, H.X. Dai, J. Catal. 332 (2015) 13–24.